Available online at www.sciencedirect.com
ScienceDirect
Journal of Electron Spectroscopy and Related Phenomena 163 (2008) 28–39
JOURNAL OF ELECTRON SPECTROSCOPY and Related Phenomena
www.elsevier.com/locate/elspec

The hemispherical deflector analyser revisited II. Electron-optical properties

E.P. Benis [a,*], T.J.M. Zouros [a,b]

[a] *Institute of Electronic Structure and Laser, P.O. Box 1385, 71110 Heraklion, Crete, Greece*
[b] *Department of Physics, University of Crete, P.O. Box 2208, 71003 Heraklion, Crete, Greece*

Received 29 November 2007; received in revised form 31 January 2008; accepted 2 February 2008
Available online 13 February 2008

Abstract

Using the basic spectrometer trajectory equation for motion in an ideal $1/r$ potential derived in Eq. (101) of part I [T.J.M. Zouros, E.P. Benis, J. Electron Spectrosc. Relat. Phenom. 125 (2002) 221], the operational characteristics of a hemispherical deflector analyser (HDA) such as dispersion, energy resolution, energy calibration, input lens magnification and energy acceptance window are investigated from first principles. These characteristics are studied as a function of the entry point R_0 and the nominal value of the potential $V(R_0)$ at entry. Electron-optics simulations and actual laboratory measurements are compared to our theoretical results for an ideal biased paracentric HDA using a four-element zoom lens and a two-dimensional position sensitive detector (2D-PSD). These results should be of particular interest to users of modern HDAs utilizing a PSD.

PACS: 07.81.+a

Keywords: Electron spectroscopy; ESCA; Hemispherical analyser; Paracentric hemispherical analyser; Fringing fields

1. Introduction

This article is the second part of an in depth investigation focusing on the study of the orbits of non-relativistic charged particles inside a hemispherical deflector analyser (HDA), as well as on the electron-optical properties and optimal operation characteristics of the HDA. The general case of a biased paracentric HDA, i.e., an HDA whose entry is biased at a nominal voltage $V(R_0) \neq 0$ and is paracentric lying at a radial position $R_0 \neq \bar{R} = (R_1 + R_2)/2$, where R_1 and R_2 are the inner and outer radii of the HDA, respectively, is considered. The conventional HDA treated in the literature to date has typically $V(R_0) = 0$ and $R_0 = \bar{R}$. Interest in such a biased paracentric HDA has been prompted by recent articles [1–9] in which electron-optical simulations demonstrated improved focusing and therefore energy resolution for such an HDA. The nature of the effect is attributed to the strong fringing fields at entry. Towards the investigation of this effect, we initially proceed with studying the trajectories of a charged particle in an *ideal* biased paracentric HDA, i.e, an HDA free of fringing fields.

Thus, in the first review article [10,11] (from here on referred to as paper I), we gave a general treatment of charged particle motion in the *ideal* potential $\tilde{V}(r) = -k/r + c$. The general trajectory equations were obtained in analytic form for r as a function of the deflection angle ω and the launching angle α. In our treatment, the reference (or principal) ray describes an elliptical trajectory starting at $r(\omega = 0) = R_0$ biased at $\tilde{V}_0 \equiv V(r(\omega = 0) = R_0)$ and exiting after deflection through $\Delta\omega = \pi$ at $r(\omega = \pi) = R_\pi$ (see Fig. 3 and Eqs. (90) and (93) in paper I). Conventional HDA trajectory equations [12–18] can be readily recovered as the special case where $R_0 = R_\pi = \bar{R}$ and $\tilde{V}_0 = V_p$, where V_p is the pre-retardation plate voltage of the analyser. The finite potential at the HDA entry $\tilde{V}_0$ was also found to introduce non-negligible refraction. Thus, a formal treatment of refraction at the idealized sharp potential boundary, represented by a step function potential $V(r, \theta)$, was also included and the basic equation of the analyser was obtained as a function of either α or $\alpha^\star$, the entry angle after or prior to refraction, respectively. The form written in terms of $\alpha^\star$ (see Eq. (I101)) was found to be surprisingly simple, much simpler than the one obtained in terms

* Corresponding author. Tel.: +30 2810391127.
E-mail address: benis@iesl.forth.gr (E.P. Benis).

0368-2048/$ – see front matter © 2008 Elsevier B.V. All rights reserved.
doi:10.1016/j.elspec.2008.02.001

of α (Eqs. (I99) and (I100) in Ref. [10,11]), arguing in favor of using the form with $\alpha^\star$.

In this paper we use the basic analyser trajectory equation for motion in an ideal potential obtained in Eq. (I101) to investigate the electron-optical properties of the generalized HDA such as dispersion, energy resolution, energy calibration and energy acceptance window. We again parameterize our results in terms of the entry radius $r = R_0$ and the nominal bias at entry $\tilde{V}_0$. Our results are also compared to electron-optics simulations using the popular ion optics package SIMION [19–21] and to actual laboratory measurements using our own biased paracentric HDA [22–24]. Both SIMION results and real measurements include the effects of the strong fringing fields, whose effects on the electron-optical properties of the HDA are further discussed.

The reader is referred to paper I for the detailed definitions and descriptions of the various variables and parameters introduced. Here we maintain the same notation. For convenience, a definition list of the symbols used here along with their values for our own HDA are given in Table A.1 of the Appendix A.

2. Focusing and dispersive properties of an ideal $1/r$ potential

The focusing properties of an ideal HDA have already been discussed in many excellent treatments [12–18]. Here we give a brief but generalized [14] approach. A basic optical layout of the spectrograph is shown in Fig. 1. A beam of charged particles emanates from a source of dimension d_s at a pencil angle $\Delta\alpha_s$ defined by the lens pupil entry d_p and its distance l from the source. The source (object) is focused by the lens onto the HDA entry plane having a dimension Δr_0 (image) smaller than the physical opening d_0 of the HDA entry aperture (for 100% transmission). Pre-retardation changes the energy of the central ray from T at the source to t just prior to HDA entry. The image Δr_0, which is associated with the maximum HDA entry half-angle $\alpha^\star_m$ and α_m (after refraction), is finally imaged after dispersion at the exit plane of the HDA and is detected by a 2D-PSD.

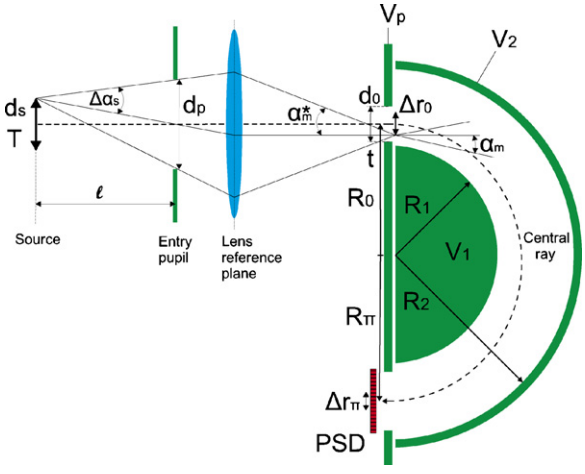

Fig. 1. Schematic geometry of typical HDA spectrograph equipped with a focusing/deceleration lens system and a 2D-PSD. The drawing has been simplified by approximating the (thick) lens by a thin lens. The vertical dimensions are particularly enhanced.

Since the HDA focusing properties can be studied from the ray trace on the exit plane [8,9,25], an expression which gives the position of the particle at the exit, as a function of its position and direction at the entry and its reduced pass energy τ is needed. This equation was derived in detail in paper I [10,11] (see Eq. (I102)) to be:

$$r_\pi = -r_0 + \frac{R_0\,(1+\xi)}{1+(\xi/\gamma)\,(1-\tau\,\cos^2\alpha^\star)}, \quad \text{(ideal HDA)} \qquad (1)$$

where (from I) r_0 and r_π are the entry and exit radii, respectively, of the particle trajectory. $\xi \equiv R_\pi/R_0$ is the paracentricity of the HDA, with R_0 and R_π the entry and exit radius of the principal trajectory, respectively. In practice, we shall always take R_π to be the mean radius of the HDA, i.e., $R_\pi = \bar{R} = (R_1 + R_2)/2$, however the symbol R_π is maintained throughout for generality. A charged particle having an initial energy T is decelerated prior to dispersion through the HDA to a pass energy of t, so that $t \equiv T - q\,V_p$. w is the nominal "tuning" energy, i.e., the energy of the principal trajectory, after preretardation. Thus, the reduced pass energy is defined as $\tau \equiv t/w$. Finally, γ is defined such that $q\,\tilde{V}(R_0) = (1-\gamma)\,w$. Note that, for a conventional HDA, $\tilde{V}(R_0) = 0$ and $R_0 = R_\pi$, so that $\xi = 1$ and $\gamma = 1$. Eq. (1) is known [26] as the *basic equation* of the spectrograph.

For an *ideal* biased HDA one also needs to consider particle refraction at the HDA entry, as discussed in detail in I. In our step potential model presented in I, refraction was found to result in a change of both kinetic energy (Eq. (I B.21)) and angle (Eq. (I B.22)) as the particle crosses the entry plane from a potential $V = 0$ to one of $V = V(r_0)$. Thus, a particle with kinetic energy $K^\star = t$ and angle $\alpha^\star$ prior to refraction at entry, will have after refraction, an energy $K = t - q\,\tilde{V}(r_0)$ and angle given by $\sin\alpha = \sqrt{t/K}\,\sin\alpha^\star$. For $t = w$ and $r_0 = R_0$, we note that $K = w - q\,\tilde{V}_0 = \gamma\,w$ and therefore $\alpha^\star \approx \gamma\,\alpha$ in the small angle approximation. Thus, for $\gamma > 1$, $K > K^\star$ and $\alpha < \alpha^\star$, the particle will in general be accelerated to larger kinetic energies and refracted to smaller angles within the HDA. These changes will influence somewhat the overall performance of the HDA.

Next, we study the basic focusing and dispersion properties of an *ideal* hemispherical spectrograph based on Eq. (1). The effects of the strong fringing field [1,6–9] are only discussed in as much as the results obtained for the ideal HDA disagree with comparisons to SIMION simulations and laboratory measurements.

2.1. Magnification, dispersion and angular aberrations

In general, the Taylor expansion of the change in exit radial position Δr_{exit} up to first order in energy change and up to second order in the angular terms takes the unique form for an electrostatic analyser given by [12–14,26]:

$$\Delta r_{exit} \equiv \mathcal{M}\Delta r_{entry} + D\frac{\Delta\tau}{\tau} + P_1\alpha^\star + P_2\alpha^{\star 2} + \ldots \qquad (2)$$

In particular, using the symbols introduced here for the HDA and after a deflection of 180° we may identify r_{exit} with r_π and

r_{entry} with r_0 [2]:

$$\Delta r_\pi \equiv r_\pi(r_0 + \Delta r_0, \tau + \Delta\tau, \alpha^\star) - r_\pi(r_0, \tau, \alpha^\star = 0)$$
$$= \mathcal{M}\Delta r_0 + D\frac{\Delta\tau}{\tau} + P_1\alpha^\star + P_2\alpha^{\star 2}, \tag{3}$$

where it can be readily shown using Eq. (1) that for an ideal HDA

$$\mathcal{M} = -1 \tag{4}$$

$$D = \frac{\tau(1+\xi)}{\gamma[1+(\xi/\gamma)(1-\tau)]^2} R_\pi \tag{5}$$

$$P_1 = 0 \tag{6}$$

$$P_2 = -D. \tag{7}$$

Here $\mathcal{M}$ is the HDA linear magnification, D the characteristic dispersion length and P_2 the polar angular aberration or trace width [12]. It is seen that the magnification $\mathcal{M}$ is always a constant, inverting the image, while the polar aberration term P_2 is always equal and opposite to the dispersion length D. These properties are thus seen to be generic of any *ideal* HDA, being independent of the type of central trajectory chosen (this includes both conventional and paracentric HDAs).

In cases where the spectrum is obtained at constant tuning energy (a part of the spectrum is recorded simultaneously over the PSD area) the dispersion length D can be defined [13,14,27] as the magnitude of the image displacement caused by a slight change in the initial pass energy t, divided by the relative energy change, for the same initial pass energy:

$$D \equiv \tau\left[\frac{\partial r_\pi}{\partial\tau}\right]_{r_\pi,\tau,\alpha^\star=0}, \tag{8}$$

from which Eq. (5) is obtained directly by differentiation of r_π as given by Eq. (1).

In Fig. 2, the dispersion D is plotted as a function of the reduced pass energy τ and the biasing parameter γ for different values of ξ. The dispersion length D is seen to be a universal function of the reduced pass energy τ and thus will vary across the length of the PSD with energy. In more detail, an increase in the particle's reduced pass energy τ, corresponds to an increase in the magnitude of the semi-major axis of its elliptical orbit inside the HDA (see Eqs. (I76) and (I88)) and therefore to an increase of the dispersion length. The increase of D with increasing paracentricity ξ at constant γ ($\tilde{V}_0$) directly reflects the geometrical increase of the dispersion length (increase in R_π). Finally, an increase in γ is equivalent to a further acceleration of the particles inside the HDA which directly leads to a decrease of the dispersion length D.

D is not affected neither by the quality of focusing at the entry of the HDA nor by the refraction corrections since it is defined for trajectories with $\alpha^\star = \alpha = 0$ [28,10,11]. The above affect only the focusing properties of the HDA and therefore its energy resolution which, however, primarily depends on the dispersion length. Thus, the energy resolution can be optimized by controlling the dispersion through the electrostatic field and geometry parameters γ and ξ, respectively.

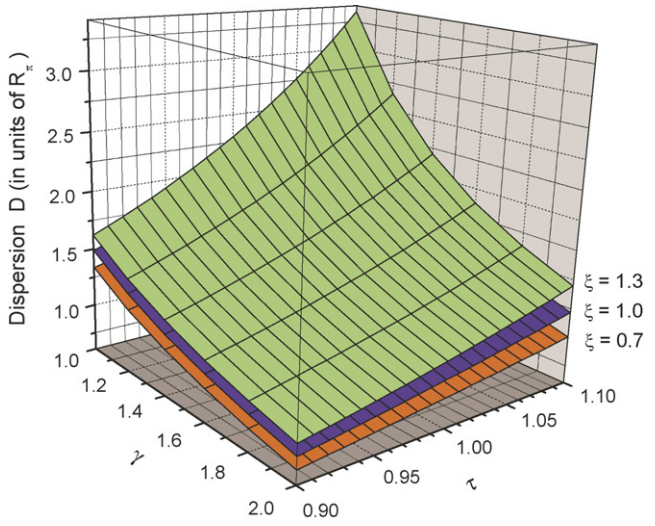

Fig. 2. The characteristic dispersion length D in units of R_π as a function of the reduced pass energy τ and the biasing parameter γ for different values of ξ. It is seen that for the same $\gamma(\tilde{V}_0)$ the dispersion D marginally increases with increasing ξ (increasing paracentricity).

2.2. Energy resolution

A hemispherical spectrograph with PSD will have a minimum spatial resolution Δr_π along the dispersion direction. For a slit spectrograph, Δr_π is the exit slit width along the dispersion direction. Thus, the spectrograph base energy resolution $\mathcal{R}_B$ will be the maximum energy spread, in the energy of the analysed particles that make it into Δr_π, centered at r_π, from anywhere within Δr_0, for any permissible angle $\alpha^\star$. Using Eq. (3), the base resolution $\mathcal{R}_B$ is written as [29,30]:

$$\mathcal{R}_B = \frac{\Delta t}{t} = \frac{\Delta\tau}{\tau} = \frac{\Delta r_\pi + \Delta r_0}{D} + \alpha^{\star 2}. \tag{9}$$

Depending on the HDA parameters, the analysed line shape very often will have a long tail, and thus the resolution at FWHM is usually smaller or equal to half the base width [15,30], i.e., $\mathcal{R}_{BFWHM} \leq \mathcal{R}_B/2$. In systems with a preretardation stage, it is the overall base resolution $\Re_B \equiv (\Delta T/T)$ of the spectrograph that is of primary importance. Using Eq. (I6), $\Re_B$ is written:

$$\Re_B \equiv \frac{\Delta T}{T} = \frac{\Delta\tau}{\tau}\left(\frac{\tau}{\tau + F - 1}\right). \tag{10}$$

A focusing and deceleration system of lenses is usually added at the entry of a spectrograph to provide control over the optical properties of the charged particle beam prior to energy analysis [31,16,32]. In this case, for conjugate object-image pairs, the Helmholtz–Lagrange law requires [33,27]:

$$|M_L| \cdot |M_\alpha| = \sqrt{\frac{T}{t}} = \sqrt{\frac{\tau + F - 1}{\tau}}, \tag{11}$$

where $|M_L| = \Delta r_0/d_s$ and $|M_\alpha| = \alpha^\star_m/\Delta\alpha_s$ are the linear and angular lens magnification terms, respectively.

For paraxial optics, $\Delta\alpha_s = d_p/(2l)$, where l is the mean distance of the object (target) to the entry of the lens and d_p is the diameter of the lens entry aperture (see Fig. 1). The entry angle

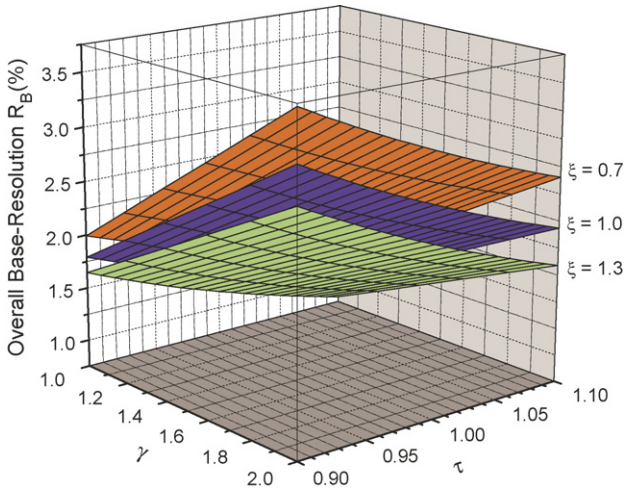

Fig. 3. Overall base-resolution as a function of the reduced pass energy τ and γ, for different ξ values. In all three plots, the lens linear magnification and the deceleration factor were set to unity, i.e., $|M_L| = 1$, $F = 1$, respectively. Note the small improvement in energy resolution at constant γ for increasing values of ξ.

$\alpha^{\star}_{m}$ may be written as:

$$\alpha^{\star}_{m} = \frac{d_p}{2\,l\,|M_L|}\sqrt{\frac{\tau + F - 1}{\tau}}. \tag{12}$$

Using Eqs. (5), (9), (12) and (10) gives:

$$\Re_B = \frac{|M_L| d_s + \Delta r_\pi}{D} \cdot \frac{\tau}{(\tau + F - 1)} + \left(\frac{d_p}{2\,l\,|M_L|}\right)^2. \tag{13}$$

Eq. (13) shows that the resolution for *fixed* lens magnification $|M_L|$ cannot be improved indefinitely by increasing the deceleration factor F, but is eventually limited by the term $[d_p/(2\,l\,|M_L|)]^2$ due to the angular term $\alpha^{\star 2}_{m}$ in the resolution expression (Eq. (9)).

In Fig. 3, a three-dimensional graph shows the overall base resolution as a function of the reduced pass energy τ and γ, for different values of ξ (see Eq. (13)). The lens linear magnification and the deceleration factor were set to unity. Fig. 3 clearly shows the slight improvement in resolution with increasing values of paracentricity ξ. This of course is a direct result of the increase of the dispersion D with increasing values of ξ, already noted previously. Clearly, it is unrelated to the reported improvement of resolution in a real paracentric HDA [1,6,7] due to the improved focusing effects introduced by the strong fringing fields of a real paracentric HDA, affecting the angular aberration term (second term in Eq. (9)).

2.2.1. *Optimum lens magnification for highest resolution*

The dependence of the energy resolution on the quality of the focusing at the HDA entry, described so far by the term $|M_L|$, is not straightforward as can be clearly seen in Eq. (13). However, it is evident that there should be an optimum value for $|M_L|$ that minimizes $\Re_B$ [2]. Thus, since the lens voltages are usually set with respect to the principal trajectory, we set $\tau = 1$ in Eq. (13)

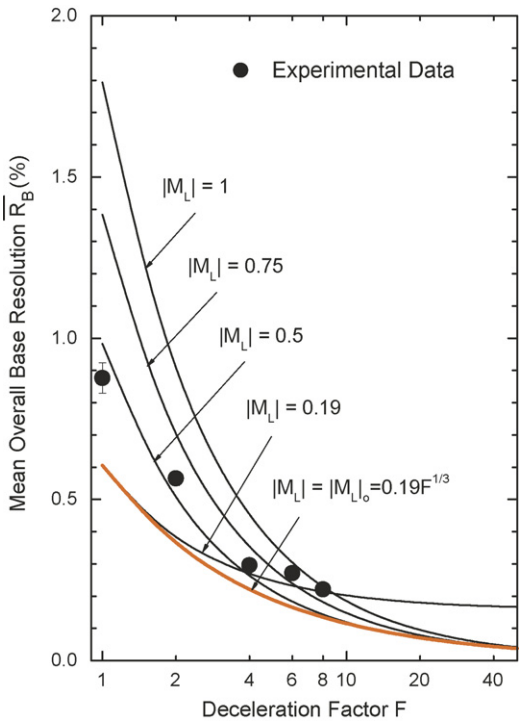

Fig. 4. Plot of the mean overall base resolution $\bar{\Re}_B$ (Eq. (14)) as a function of the deceleration factor for lens magnification $|M_L|$ values of 1, 0.5, 0.75, 0.19 and optimum value $|M_L|_o = 0.19\,F^{1/3}$. Clearly, for small values of F it is important to be near the optimum lens magnification. The data points are from measured resolution values taken in the laboratory with our HDA.

defining the mean overall base resolution $\bar{\Re}_B$ as:

$$\bar{\Re}_B \equiv \Re_B(\tau = 1) = \frac{(|M_L| d_s + \Delta r_\pi)}{\bar{D}\,F} + \left(\frac{d_p}{2\,|M_L|\,l}\right)^2, \tag{14}$$

where $\bar{D} \equiv D(\tau = 1) = (1 + \xi)\,R_\pi/\gamma$ is the mean dispersion. Setting the first derivative of $\bar{\Re}_B$ with respect to $|M_L|$ to zero we obtain after some straightforward algebra, the optimum value for $|M_L|$ [2]:

$$|M_L|_o = \left[\frac{1}{2}\left(\frac{\bar{D}\,F}{d_s}\right)\left(\frac{d_p}{l}\right)^2\right]^{1/3}. \tag{15}$$

Substituting $|M_L|_o$ back into Eq. (14) the mean overall optimum base resolution is found to be [2]:

$$\bar{\Re}_{Bo} = \bar{\Re}_B(|M_L|_o) = \frac{\Delta r_\pi}{\bar{D}\,F} + \frac{3}{2^{2/3}}\left(\frac{d_p}{2\,l}\frac{d_s}{\bar{D}\,F}\right)^{2/3}. \tag{16}$$

In Fig. 4, the mean overall base resolution is plotted as a function of the deceleration factor F. For the parameters of our particular setup it was found that $|M_L|_o = 0.19\,F^{1/3}$. A comparison between the above cases, indicates that substantial gains can be made in energy resolution by initially fine tuning $|M_L|$ at $F = 1$. At higher values of F the resolution becomes increasingly insensitive to changes in $|M_L|$. Also, it is evident that optimum resolution does not only depend on the quality of the focusing at the entrance of the HDA, i.e., a constant value of $|M_L|$, but on the deceleration factor as well. Thus, for each deceleration factor F the value of $|M_L|$ for the optimum reso-

lution should be attained, as it is clearly seen for the cases of $|M_L| = 0.19$ and $|M_L|_o = 0.19\,F^{1/3}$.

A possible overestimation in the above study is that the energy resolution is seen to keep improving with increasing F, assuming that the lens magnification is also adjusted according to Eq. (15). At this point we shall consider the lens as an ideal lens allowing the magnification to be treated as a free parameter. However, when $|M_L| > d_0/d_s$ (see Fig. 1), the virtual aperture size Δr_0 will exceed the real size aperture of the HDA entry d_0. Thus, charged particle transmission losses through the lens begin to occur, setting a limit to the maximum useful value of M_L, and therefore to the minimum possible resolution attainable at 100% transmission. However, for virtual entry HDAs, d_0 is usually much larger than Δr_0, so an attenuation in the transmission will occur only at very high F values at which however, other limiting parameters not considered in our ideal HDA treatment could become important (e.g., aberrations, external magnetic fields, etc.). The experimental data points shown are from measured resolution values taken in the laboratory with our paracentric HDA and will be further discussed below.

2.2.2. Spectrograph design criterion

An important feature in designing a spectrograph in general, is that the shape of the transmission function not be significantly affected by the angular abberation term in Eq. (9). In order to reduce the tailing of the line shape, Kuyatt and Simpson proposed the following criterion for the ratio χ of the angular term to the dispersion term [17].

$$\chi \equiv \frac{\alpha_m^{\star\,2}}{(\Delta r_\pi + \Delta r_0)/D} \leq \frac{1}{2}. \tag{17}$$

This value seems to have been adopted as the standard [16] in the design of HDAs with slits operating in the non-deceleration mode. Using the optimized conditions for the energy resolution described above, i.e, $|M_L| = |M_L|_o$ with Eq. (17), the mean optimized ratio $\bar{\chi}_o = \chi(\tau = 1, |M_L| = |M_L|_o)$ is written as [2]:

$$\bar{\chi}_o = \frac{1}{2} - \left(2 + \frac{2[(1/2)((d_s/\bar{D}\,F)(d_p/l))^2]^{1/3}}{(\Delta r_\pi/\bar{D}\,F)}\right)^{-1}. \tag{18}$$

In Fig. 5, $\bar{\chi}$ is plotted as a function of F for various linear magnifications $|M_L|$, including the case of resolution-optimized condition $|M_L| = |M_L|_o$ that corresponds to the mean optimized ratio $\bar{\chi}_o$. We note that $\bar{\chi}_o$ always fulfills the Kuyatt–Simpson criterion contrary to other choices of constant linear magnification. Therefore, the long standing design criterion standard for spectrometers is seen to be valid for HDA systems incorporating a focusing/deceleration lens system, allowing for maintaining the imaging properties at large deceleration factors. Finally, the seemingly adhoc value of 1/2 in the Kuyatt–Simpson criterion is seen to arise naturally as the limit of $\bar{\chi}_0$ for $F \to \infty$ [2].

2.3. Energy calibration

The energy calibration of a spectrograph establishes the relation between exit particle position and its initial kinetic energy.

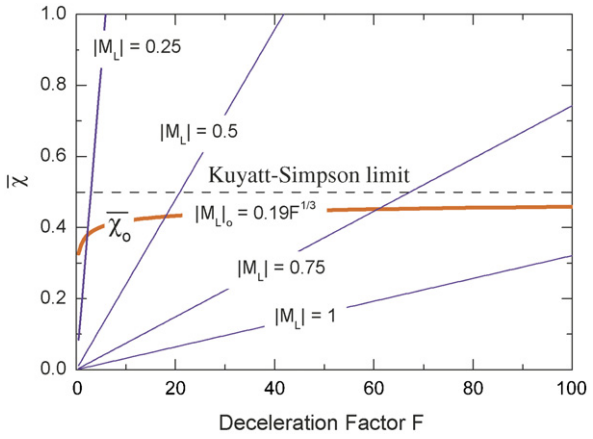

Fig. 5. $\bar{\chi}$ ratio of angular to dispersion resolution terms plotted as a function of the decelerating factor F for various values of the linear magnifications $|M_L|$. Note that for the resolution optimized conditions $|M_L| = |M_L|_o$, $\bar{\chi}_o$ is always below the Kuyatt–Simpson limit, shown by the dashed line.

In the laboratory, the particle position is known from the channel number i on the PSD where the particle hits. Therefore a relation between the initial kinetic energy and the channel number i, rather than the exit position, must be established. Here, the above relationship is derived theoretically, for a generalized spectrograph. Initially, it is assumed that the position along the PSD, r_{π_i}, depends linearly on the channel number i

$$r_{\pi_i} = G + H\,i. \tag{19}$$

Constants G and H will in general depend on the electronic setup. Assuming, n to be the total number of channels available, there will always be channels i_{min} and i_{max} which will correspond to the limiting positions along the PSD of $r_\pi(\text{min}) = R_\pi - d_{PSD}/2$ and $r_\pi(\text{max}) = R_\pi + d_{PSD}/2$, respectively, such that

$$R_\pi - \frac{1}{2}d_{PSD} = G + H\,i_{min} \tag{20}$$

$$R_\pi + \frac{1}{2}d_{PSD} = G + H\,i_{max}, \tag{21}$$

where d_{PSD} is the diameter of the active PSD area centered at R_π. Eqs. (20) and (21) are solved for the parameters G and H and upon substituting back into Eq. (19), the position calibration equation reads

$$r_{\pi_i} = R_\pi - \left(\frac{1}{2} + \frac{i_{min}}{n}\right) d_{PSD} + \frac{i}{n}\,d_{PSD}, \tag{22}$$

where it was assumed that the center of the PSD at R_π corresponds to the center of the channel range (e.g. $n/2$), and $n \equiv i_{max} - i_{min}$. Then, assuming the averages $\langle\alpha^\star\rangle = 0$ and $\langle r_0\rangle = R_0$, the averaged reduced pass energy $\langle\tau\rangle$ of the analysed particles can be related to the channel number via Eq. (1) as:

$$\langle\tau\rangle = \frac{\gamma(\langle r_\pi\rangle/R_0) + (1 - \gamma + (\langle r_\pi\rangle/R_0))\xi}{(1 + (\langle r_\pi\rangle/R_0))\xi}. \tag{23}$$

Upon substitution of $\langle r_\pi\rangle$ with r_{π_i} from Eq. (22) and $\langle\tau\rangle$ with τ_i gives the exact energy versus channel number calibration

relation for an ideal HDA

$$\tau_i = \frac{1+\xi+(s/R_\pi)(\gamma+\xi)(i-i_0)}{1+[1+(s/R_\pi)(i-i_0)]\,\xi}, \tag{24}$$

where $i_0 = (i_{\max}+i_{\min})/2$ is the center channel and $s = (d_{\mathrm{PSD}}/n)$ is the effective "slit" width of a single channel.

It is seen that the relationship between the reduced pass energy τ and the channel number i is in general *not linear*. When the quantity $\delta_i \equiv (s/R_\pi)(i-i_0)$ is smaller than 1, as in most cases, a power expansion of the denominator of Eq. (24) is justified yielding

$$\tau_i \approx A + B\,i + C\,i^2, \tag{25}$$

where

$$A = 1 - \frac{s\,i_0\gamma[s\,i_0\xi + R_\pi\,(1+\xi)]}{[R_\pi\,(1+\xi)]^2} \tag{26}$$

$$B = \frac{s\,\gamma\,[2s\,i_0\,\xi + R_\pi(1+\xi)]}{[R_\pi(1+\xi)]^2} \tag{27}$$

$$C = -\frac{s^2\gamma\,\xi}{[R_\pi(1+\xi)]^2}. \tag{28}$$

2.4. Energy acceptance window

For an exit slit spectrometer the energy acceptance window is just the base energy width. For the case of a spectrograph using a PSD instead with effective diameter d_{PSD} the energy acceptance window $\Delta T_{\mathrm{window}}$ is defined [18] as the energy range which can be simultaneously recorded on the PSD.

Using Eq. (1) and assuming the averaged entrance angle $\langle\alpha^\star\rangle = 0$ and $\langle r_0\rangle = R_0$, the reduced pass energy is related to position relation via:

$$\tau = \frac{r_\pi(\gamma+\xi) - R_\pi(\gamma-1)}{R_\pi + r_\pi\,\xi}. \tag{29}$$

Assuming that the end points of the PSD are at $R_\pi \pm d_{\mathrm{PSD}}/2$ achieved at the energy acceptance limits $\tau_{\max}$ and $\tau_{\min}$, the reduced energy acceptance window $\Delta\tau_{\mathrm{window}} = \tau_{\max} - \tau_{\min}$ is obtained from Eq. (29):

$$\Delta\tau_{\mathrm{window}} = \frac{[d_{\mathrm{PSD}}/(R_\pi\,(1+\xi))]\,\gamma}{1-(\xi/2)^2[d_{\mathrm{PSD}}/(R_\pi\,(1+\xi))]^2} \tag{30}$$

$$\approx \frac{\gamma}{1+\xi}\,\frac{d_{\mathrm{PSD}}}{R_\pi}. \tag{31}$$

In systems with a deceleration stage, it is the quantity $\Delta T_{\mathrm{window}} = T_{\max} - T_{\min}$ which is of importance, since it depends on the deceleration factor F. Using Eq. (I6), $\Delta T_{\mathrm{window}}$ is written as:

$$\Delta T_{\mathrm{window}} = \Delta\tau_{\mathrm{window}}\,\frac{W}{F}. \tag{32}$$

The energy acceptance window $\Delta T_{\mathrm{window}}$ is inversely proportional to the deceleration factor F, as is the energy resolution to first order in $\alpha^\star$ (see Eq. (9)).

The dependence of $\Delta\tau_{\mathrm{window}}$ on γ may be explained directly from the fact that γ acts as an acceleration/deceleration factor. From conservation of energy the central ray must have a new energy w' at R_0 such that $w' + qV_0 = w + qV_{\mathrm{p}} = W$. Using the definition of γ from Eq. (I3), we obtain $w'/w = \gamma$. Thus, for $\gamma > 1$, the particle is further accelerated, so that a central ray with initial energy W ends up having a pass energy w' at R_0 such that $w' = (\gamma/F)W$. The ratio γ/F is thus seen to be the overall deceleration/acceleration factor instead of $1/F$.

3. The paracentric HDA: measurements and SIMION simulations

This study of the focusing and dispersive properties of the paracentric HDA was primarily prompted by the use of such a spectrograph in zero-degree Auger projectile spectroscopy (ZAPS) [34–36]. ZAPS is a well known technique in fast ion–atom collisions allowing for high resolution measurements by utilizing the minimization of the kinematic broadening at zero-degrees with respect to the beam direction. Recent reviews of the technique can be found in [34,36]. An example of high resolution ZAPS spectrum taken with our ZAPS setup is shown in Fig. 6 for the collision system of 17.97 MeV N^{4+} + He. A deceleration factor of $F = 4$ was adequate to resolve the N^{3+}KLL lines. The ZAPS setup, a schematic of which is shown in Fig. 7, has already been described to a certain extent [37,22,23].

The experimental study of the spectrograph's focusing and dispersive properties was performed using the 21.6 MeV F^{8+} + H_2 collision system. The advantage of this system is that the spectrum consists of a broad Binary Encounter electron (BEe) peak [38,22,23,36] with a single Auger (the $2p^2\,{}^1D$) lying on top of it, as illustrated in Fig. 8. The Auger peak was used for studying the energy resolution, by recording the FWHM of the peak at different experimental conditions. The BEe was used for the energy window study and also for cross section normaliza-

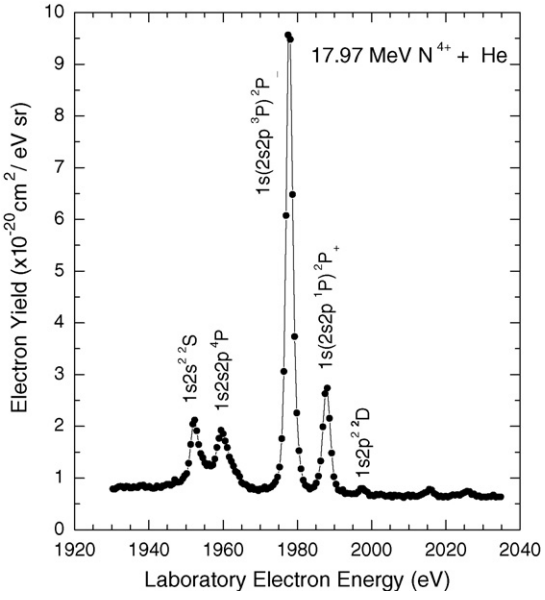

Fig. 6. High resolution Auger spectra for the collision system of 17.97 MeV N^{4+} + He obtained with the paracentric spectrograph. The data were recorded at zero-degrees with respect to the beam direction. A deceleration factor of $F = 4$ was adequate to resolve the N^{3+}KLL lines.

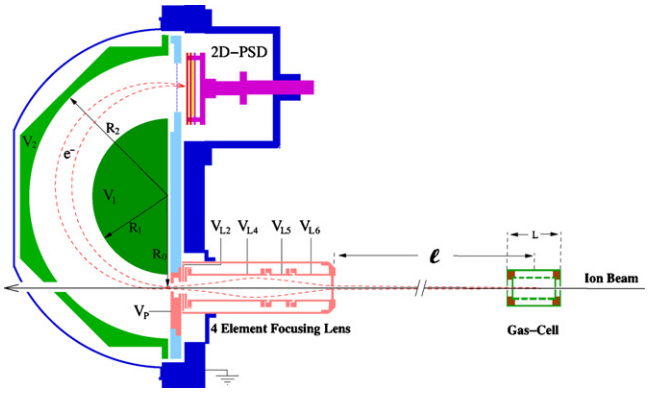

Fig. 7. Schematic of the ZAPS experimental setup. Note the asymmetric (paracentric) position of the entry aperture on the HDA. The voltage notation corresponds to the different electrodes.

tion purposes [39,40,36,22,23]. In addition, an electron gun was used to obtain the energy calibration.

The study of a realistic HDA including fringing fields was also performed using the electron-optics package SIMION [20]. Thus, the whole experimental setup was designed in SIMION. Special care was given to maintain the ratio of the distance between the lens elements to lens diameter at 1/10. This value corresponds to our lens geometry and is also very common in lens design [33]. A detailed design of our lens is shown in Fig. 9.

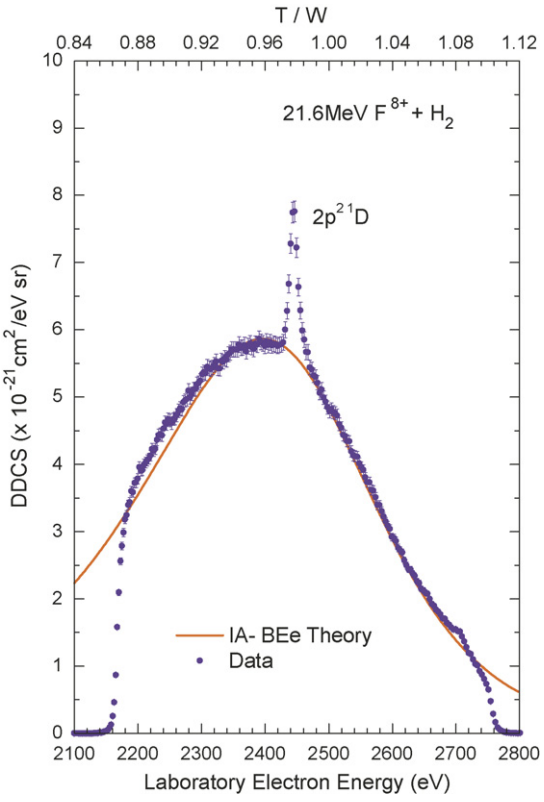

Fig. 8. Typical zero-degree electron spectrum of the 21.6 MeV $F^{8+} + H_2$ collision system obtained with the paracentric spectrograph. Deceleration factor $F = 1$. The $2p^2\,^1D$ Auger peak superimposed on the broad Binary Encounter electron (BEe) peak [22,23] is well pronounced. The abrupt reduction of the electron yield at the sides corresponds to the limits of the PSD detector.

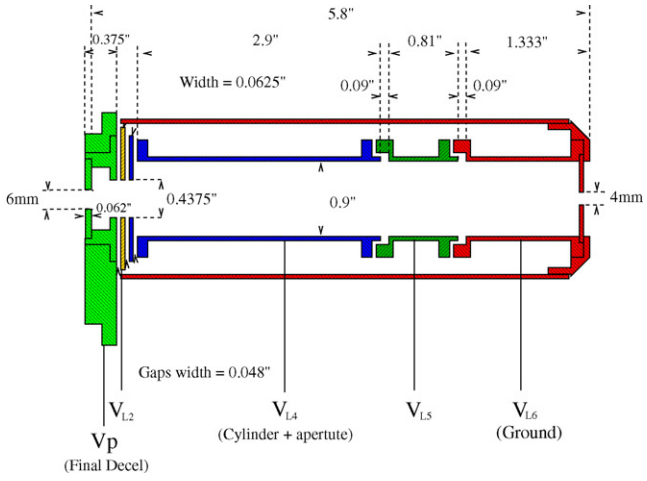

Fig. 9. Detailed design of the lens used with the HDA.

The analyser was tuned to each electron energy, using the voltages given by Eq. (I109). The lens voltages were adjusted close to the experimental values so that minimum energy resolution conditions were achieved. A small number of electrons (70) were flown from the target (gas cell) area at appropriate energies, covering the whole solid angle, thus simulating the experimental conditions. The electron-optical properties of the HDA could then be studied from their trace on the PSD.

The present experimental arrangement did not allow for mounting the lens at different entry values R_0 and therefore for comparing the resolutions at different values of R_0, which limited the experimental study to just $R_0 = 82.6$ mm and $\xi = 1.230$. Thus, all subsequent SIMION or ideal theoretical calculations presented here were performed with these values. Moreover, the focusing lens optimum voltage values were empirically determined in all cases, since the focusing quality (i.e., $|M_L|$) could only be indirectly inferred from the trace width of the $2p^2\,^1D$ electron Auger peak on the PSD area. Thus, a study based primarily on the minimization of the energy resolution gave for the optimal lens voltages the empirical values presented in Table 1 for various deceleration factors F. An example of the study is shown in Fig. 10 for the case of $F = 4$.

In the above studies, the value of γ used was 1.5. This is also the value for the data presented below unless otherwise stated. This value was determined by experimental studies of the optimization of the energy resolution. In Fig. 11, the mean overall base resolution is plotted as a function of γ along with the corresponding SIMION simulations and theoretical predictions for

Table 1
Optimum lens voltages determined empirically and mean overall base energy resolution $\bar{\Re}_B$ for different deceleration factors

F	V_p/W	V_{L4}/W	V_{L5}/W	$\bar{\Re}_B$ (%)
1	0	−0.45	0.92	0.88 ± 0.04
2	−0.50	−0.49	0.82	0.56 ± 0.02
4	−0.75	−0.45	0.88	0.30 ± 0.01
6	−0.83	−0.57	0.49	0.27 ± 0.01
8	−0.88	−0.24	0.65	0.22 ± 0.01

The value of V_{L2} was set equal to that of V_{L4}.

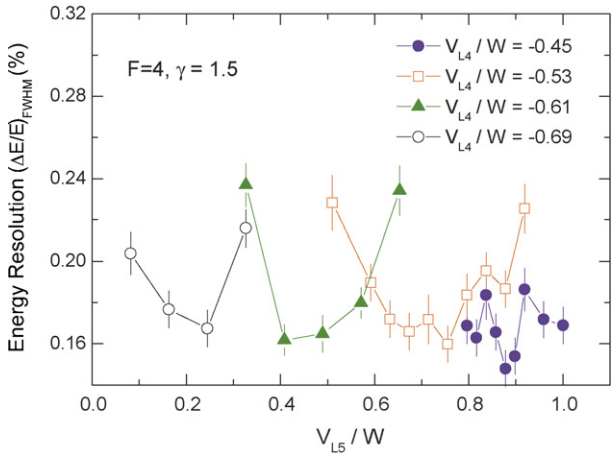

Fig. 10. Experimental energy resolution at FWHM study for deceleration factor $F = 4$. Lens voltages V_{L5} and V_{L4} were scanned over a wide range appropriate for minimizing the FWHM of the $2p^2\ ^1D$ Auger line, which was produced in collisions of 21.6 MeV $F^{8+} + H_2$.

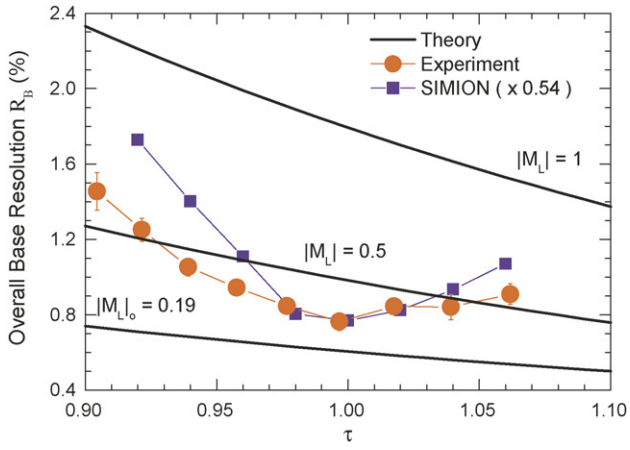

Fig. 12. Overall base resolution $\Re_B$ as a function of the reduced pass energy τ. Comparison between ideal theory, SIMION simulation and experiment. Here $F = 1$. The last two include the effects of the fringing fields.

the ideal $1/r$ field HDA. A reasonable agreement in the general behavior but not in the absolute values between measurements and SIMION calculations is evident. This behavior is solely due to the fringing fields which alter the monotonically increasing mean overall base resolution with increasing field strength as predicted for the ideal $1/r$ field. A clear minimum is evident both in data and simulations. Thus, certain values of γ are seen to be preferable for the optimization of the energy resolution, justifying the choice of $\gamma = 1.5$. Actually, as already reported [1,6,7], the paracentric entry ($\xi > 1$) along with the non-zero entry potential ($\gamma \neq 1$) can provide improved quality focusing conditions due to the presence of the large fringing fields.

It should be noted here that in realistic HDAs the biasing parameter γ refers to the *nominal* value of $\tilde{V}_0$, since $\tilde{V}_0$ can be defined only for ideal $1/r$ fields. Experimentally or in SIMION calculations, $\tilde{V}_0$, and therefore γ, should rather be considered as a control parameter for the field strength.

The mean overall base resolution $\bar{\Re}_B$ has also been studied as a function of the deceleration factor F. The data were presented in Fig. 4 in comparison to theoretical predictions for various values of the lens linear magnification $|M_L|$. The comparison is only qualitative since the actual value of $|M_L|$ cannot be determined in this setup.

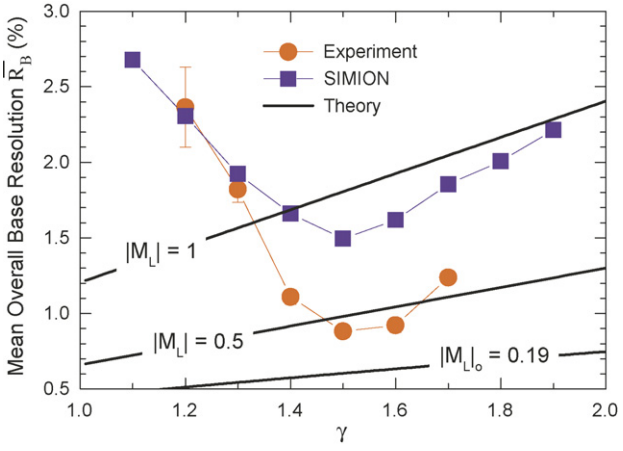

Fig. 11. Mean overall base energy resolution as a function of γ. Comparison between ideal theory, SIMION, and experiment. The last two include the effects of the fringing fields.

Very high deceleration factors allowing for high resolution studies are regularly achieved by HDA spectrometers that use very narrow exit slits. However, in these spectrometers the energy resolution is determined solely by the openings of the entry and exit slits, and the distance between them, while in the spectrograph under examination the energy resolution is controlled by the lens linear magnification factor $|M_L|$. Thus, even though the deceleration factors reported here are relatively small, the absolute energy resolution is comparable to that of HDA spectrometers using very narrow slits.

A comparison of the overall base resolution $\Re_B$ as a function of the reduced pass energy τ, describing the energy resolution over the PSD detection area, is shown in Fig. 12. A reasonable qualitative agreement between SIMION and measurements is clearly seen. Ideal potential theoretical results for different magnification factors were also plotted in order to obtain an indirect estimation of the value of $|M_L|$.

Deviations from the ideal theoretical curves is assumed to be due to effects introduced by the strong fringing fields. However, another factor that must also contribute to the deviation is the lens' chromatic aberrations. The lens voltages are set to minimize the energy resolution of the rays at the energy $T = W$. This means that other source electron energies, $T < W$ or $T > W$, will be focused either before or after the lens exit, respectively, producing images corresponding to $|M_L| > |M_L|_W$, in general, where $|M_L|_W$ is the magnification factor for the rays at $T = W$. This condition degrades the energy resolution as the edges of the PSD are approached. It should be noted however, that as F is increased and the acceptance window correspondingly decreased (see Eq. (16)) chromatic aberrations of the lens are expected to also become smaller.

In Fig. 13, the energy acceptance window $\Delta\tau_{window}$ is plotted as a function of γ. SIMION and experimental results are very similar showing a much smaller increase of the energy window

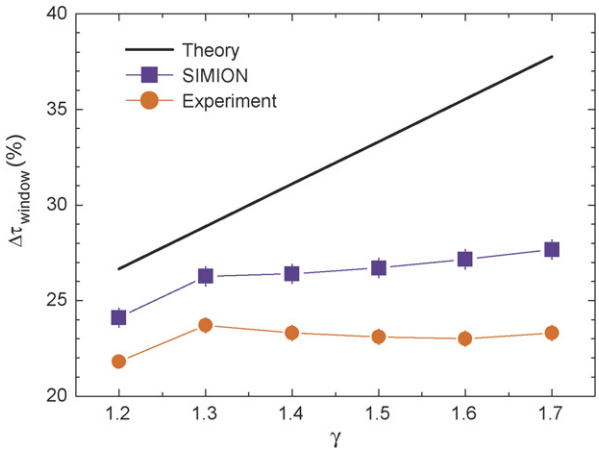

Fig. 13. Comparison of the reduced energy acceptance window $\Delta\tau_{window}$ predicted by ideal HDA theory, SIMION and experiment for the HDA under study.

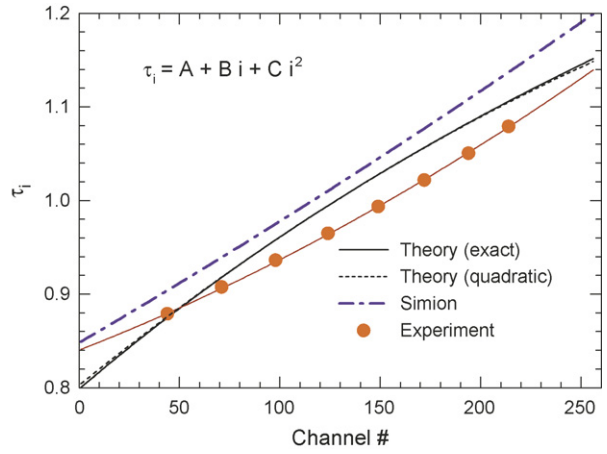

Fig. 15. Comparison of the energy calibration curves for $F = 1$ as predicted by exact ideal theory (Eq. (24)), quadratic ideal theory (Eq. (25)), SIMION and experiment. The later two include the effects of fringing fields.

with increasing γ primarily attributed to transmission losses at the edges of the PSD detection area caused by the fringing fields. The energy acceptance window $\Delta T/W$ is also plotted as a function of the inverse deceleration factor $1/F$ as seen in Fig. 14. The data are in quite good agreement with theory, as expected, since in this case focusing effects are insignificant.

In Fig. 15, the comparison of the energy calibration curves for the case of $F = 1$ is shown. Good agreement between the two theoretical models show that the quadratic model is a good approximation. The measurements and the simulations correspond to HDA tuning energies ranging from 300 to 3000 eV. The effect of the fringing fields is again evident since SIMION and experiment show similar behavior, contrary to the ideal $1/r$ case. Note the change in the sign of the curvature of the lines in SIMION and experiment compared to ideal theory. This is due to the opposite sign of the parameter C in the energy calibration relation of Eq. (25) as can be clearly seen in Fig. 16, where the parameters A, B and C of Eq. (25) are plotted as a function of γ. It is interesting to note that for increasing values of γ, C eventually goes through zero therefore resulting in a truly linear energy calibration curve. This could be of interest to further pursue as no studies have been reported.

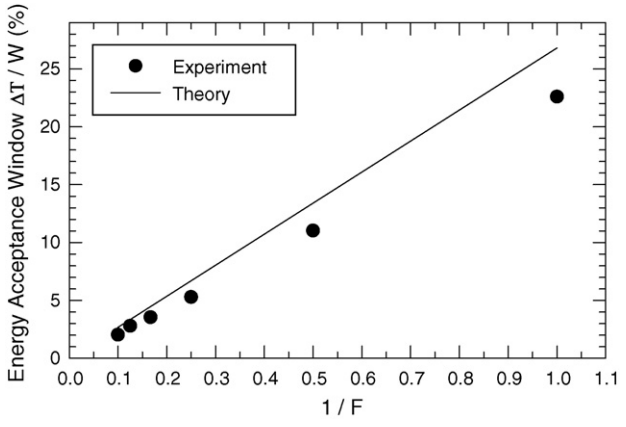

Fig. 14. Experimental energy acceptance window $\Delta T/W$ as a function of the inverse deceleration factor $1/F$.

An important factor in all spectrometers utilizing preretardation to improve energy resolution is the electron transmission as a function of the deceleration factor F. Transmission is defined as the ratio of the number of particles detected at the spectrograph exit (PSD area) over the number of particles entering the spectrograph entry (lens entry). For conventional two-stage parallel

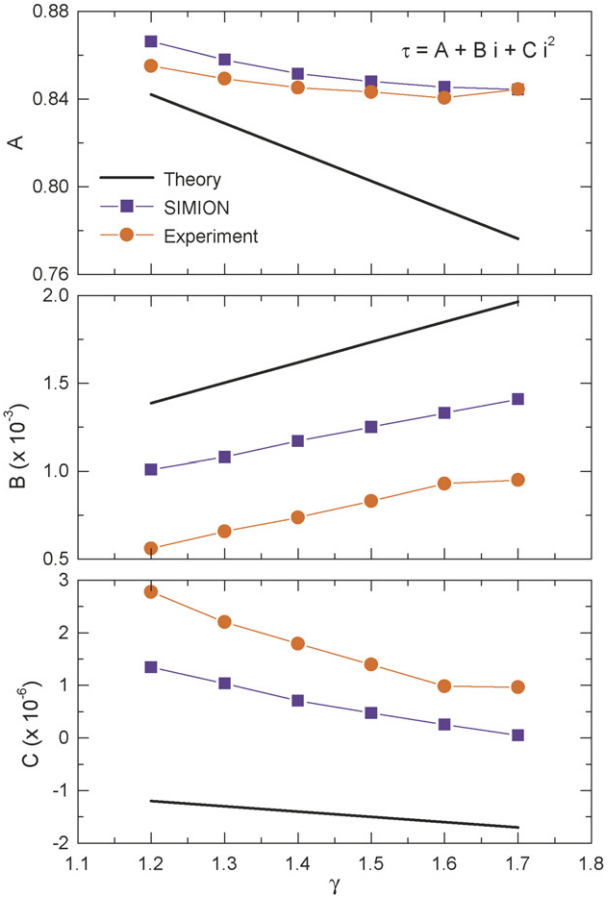

Fig. 16. The parameters A, B and C of the energy calibration relation (Eq. (25)) are plotted as a function of γ. Comparison between ideal theory, SIMION simulation and experiment.

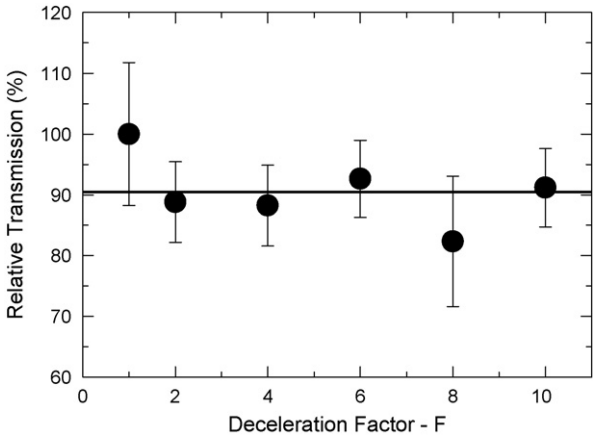

Fig. 17. The electron yield of the $2p^2\ ^1D$ line obtained in collisions of 21.6 MeV $F^{8+} + H_2$ plotted as a function of the deceleration factor F. A 90% spectrograph transmission is observed for deceleration factors up to $F = 10$.

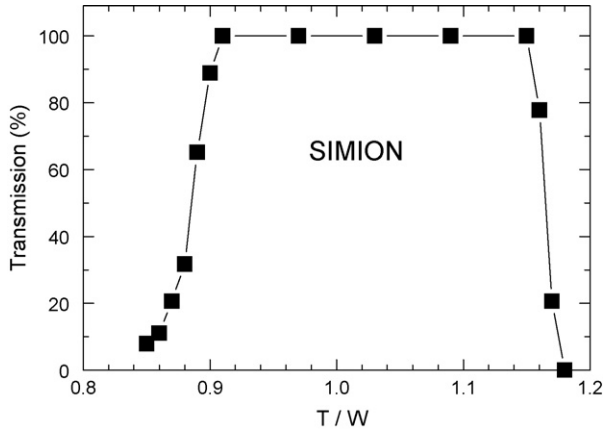

Fig. 18. SIMION study of transmission of the hemispherical spectrograph. Deceleration factor was set to $F = 1$.

plate analysers used in the field of ZAPS the overall transmission drops drastically with increasing F, practically a linear function of $1/F$ [36]. In Fig. 17, the relative electron transmission (for $F = 1$, 100% relative transmission is assumed) measured from the electron yield of the $2p^2\ ^1D$ line obtained in collisions of 21.6 MeV $F^{8+} + H_2$ (shown in Fig. 8 for $F = 1$) is plotted as a function of the deceleration factor F. The electron yield is seen to be practically constant for a factor F up to 10. This indicates that there are insignificant transmission losses, either inside the lens or inside the HDA. This is one of the advantages of using a spectrograph with focusing/decelerating lens system and virtual aperture, as large apertures can be implemented allowing for almost 100% transmission while at the same time the energy resolution is controlled by the lens magnification through Eq. (13).

Transmission is, in general, a function of the particle exit position. According to the theory of the ideal HDA, the transmission function is described by a trapezoidal form [18,12]. In principle the lens transmission can be assumed to be unity, due to the large analyser entry opening used ($d_0 = 6$ mm). Therefore the linear magnification can easily be limited to values of $|M_L| < d_0/d_s = 6/2.5 = 2.4$, even for very high deceleration factors, when proper lens voltages are applied. In principle, a value of $|M_L| \leq 2.4$ allows for deceleration factors F up to 2000 (for 100% transmission) well above the observed conditions of operation. Consequently, the spectrograph transmission should follow the trapezoidal form of the ideal HDA.

Indeed, in Fig. 18 a SIMION study of the HDA transmission is shown for the case of $F = 1$. Lens voltages were set according to the energy resolution optimization. The trapezoidal transmission function form is evident. The same trapezoidal form can be seen in the experimental data shown in Fig. 8. The data were normalized to the theory by an overall scaling factor. The agreement between theory and measurement, as well as the sudden cut-off of the spectrum at both edges justifies the trapezoidal form. It should be noted however, that the maximum absolute transmission value is determined by the two 90% transmission grids, placed at the exit of the analyser just before the PSD.

The comparative study between simulations and measurements are in general in good qualitative agreement, indicating that the SIMION ion-optics package can be a very useful tool in designing and studying charged-particle detection systems. Since the accuracy of SIMION predictions [21] was not the aim of this work, SIMION was only used as a guide to get an insight in understanding the electron-optical behavior of the generalized HDA.

4. Conclusions

The focusing and dispersive properties of the generalized HDA were studied as a function of the entry point R_0 and the nominal value of the potential at the entry $\tilde{V}_0 \equiv V(R_0)$. Analytical expressions for the dispersion, energy resolution, energy calibration and energy acceptance window were derived in the generalized case of a biased paracentric HDA spectrograph equipped with a focusing/deceleration lens system. Moreover, the energy resolution of the HDA was studied as a function of the lens linear magnification $|M_L|$, showing that there is an optimum value $|M_L|_o$ depending on geometrical factors as also on the deceleration factor F, which minimizes the energy resolution. The condition $|M_L| = |M_L|_o$ establishes a practical criterion for designing spectrographs incorporating lens focusing elements. Experimental results and simulations using SIMION were compared for energy resolution, energy calibration and energy acceptance window, in the case of $R_0 = 82.6$ mm. Comparison showed a general qualitative agreement between SIMION and experiment, which however deviate from the ideal HDA theoretical results, indicating in this way the role of the fringing fields. Our results presented here complement the theoretical description of particle trajectories presented in Ref. [10,11].

Acknowledgments

We thank Prof. Pat Richard, former director of the JRML, for his constant support and interest throughout this work. This work has received partial support from the Greek Ministry of Research and Technology and the Chemical Sciences, Geosciences and

Biosciences Division, Office of Basic Energy Sciences, Office of Science, U S Department of Energy.

Appendix A

Table A.1.

Table A.1
An alphabetical list of the most important symbols used in this paper is given for convenience together with its value for our particular biased paracentric HDA where appropriate

c	$\mathrm{V}(r) = (-k/r) + c$ (see Eqs. (I87, I105))	
d_o	diameter of HDA entry aperture (image)	6 mm
d_s	object diameter	2.5 mm
d_p	diameter of the lens entrance aperture (pupil)	4 mm
d_PSD	(active) PSD diameter	40 mm
D	HDA dispersion	
$\bar{D}$	HDA mean dispersion, $\bar{D} \equiv D(\tau = 1)$	
F	deceleration ratio, $F = W/w$	
i_max	maximum PSD channel number	226
i_min	minimum PSD channel number	32
k	$\mathrm{V}(r) = (-k/r) + c$ (see Eqs. (I86, I106))	
l	mean distance of the object to the entrance of the lens	264 mm
$\lvert M_\alpha \rvert$	lens angular magnification, $\lvert M_\alpha \rvert = \alpha^\star_\mathrm{m}/\Delta\alpha_\mathrm{s}$	
$\lvert M_\mathrm{L} \rvert$	lens linear magnification, $\lvert M_\mathrm{L} \rvert = \Delta r_0/d_\mathrm{s}$	
$\lvert M_\mathrm{L} \rvert_\mathrm{o}$	optimum lens linear magnification value (Eq. (15))	
$\mathcal{M}$	HDA linear magnification, $\mathcal{M} = -1$	
P_2	HDA polar angular aberration or trace width, $P_2 = -D$	
n	PSD number of channels	195
q	particle charge ($q = -e$ for electron)	
r_0	electron trajectory radius at HDA entry	
r_π	electron trajectory radius at HDA exit	
R_0	principal ray entry radius	82.6 mm
R_π	principal ray exit radius, $R_\pi = \bar{R}$	
R_1	HDA inner radius	72.4 mm
R_2	HDA outer radius	130.8 mm
$\bar{R}$	HDA mean radius	101.6 mm
$\mathcal{R}_\mathrm{B}$	the HDA base energy resolution, $\mathcal{R}_\mathrm{B} \equiv \Delta t/t$	
$\Re_\mathrm{B}$	HDA overall base energy resolution, $\Re_\mathrm{B} \equiv \Delta T/T$	
$\bar{\Re}_\mathrm{B}$	HDA average overall base energy resolution, $\bar{\Re}_\mathrm{B} \equiv \Re_\mathrm{B}(\tau = 1)$	
$\bar{\Re}_{Bo}$	HDA optimum average overall base energy resolution, $\bar{\Re}_{Bo} = \bar{\Re}_\mathrm{B}(\lvert M_\mathrm{L} \rvert_\mathrm{o})$	
t	particle kinetic energy (before refraction) at HDA entry	
T	particle kinetic energy far from HDA	
$V(r)$	HDA potential, $V(r) = \mathrm{V}(r) + V_\mathrm{p}$	
$\mathrm{V}(r)$	$\mathrm{V}(r) = (-k/r) + c$	
V_0	nominal voltage $V(R_0)$ (see Eq. (I3))	
V_1	nominal voltage $V(R_1)$ on R_1 (see Eq. (I109))	
V_2	nominal voltage $V(R_2)$ on R_2 (see Eq. (I109))	
V_p	biased voltage for deceleration, $V(r) = \mathrm{V}(r) + V_\mathrm{p}$	
V_L2	lens element 2 voltage ($= V_\mathrm{p}$)	
V_L4	lens elements 3 and 4 voltages	
V_L5	lens element 5 voltage	
V_L6	lens element 6 voltage (grounded)	
w	HDA tuning energy after deceleration	
W	HDA tuning energy prior to deceleration	
α	launching angle in plane of orbit	
$\Delta\alpha_\mathrm{s}$	maximum lens entrance half-angle (pencil angle)	
$\alpha^\star_\mathrm{m}$	maximum HDA entrance half-angle	
γ	HDA entry bias parameter to set V_0 (see Eq. (I3))	1.5
Δr_π	PSD spatial resolution	0.2 mm
$\Delta\tau_\mathrm{window}$	HDA energy window	
ξ	HDA paracentricity $\xi = R_\pi/R_0$	1.230
τ	reduced pass energy, $\tau = t/w$	$\sim 20\%$
χ	spectrometer design criterion	$\chi \equiv \alpha^{\star\,2}/\mathcal{R}_\mathrm{B}$
$\bar{\chi}$	$\bar{\chi} \equiv \chi(\tau = 1)$	

References

[1] E.P. Benis, T.J.M. Zouros, Nucl. Instrum. Methods Phys. Res. A 440 (2000) 462.
[2] T.J.M. Zouros, E.P. Benis, Appl. Phys. Lett. 86 (2005) 094105.
[3] T.J.M. Zouros, E.P. Benis, I. Chatzakis, Nucl. Instrum. Methods Phys. Res. B 235 (2005) 535.
[4] T.J.M. Zouros, J. Electron Spectrosc. Relat. Phenom. 152 (2006) 67.
[5] T.J.M. Zouros, J. Electron Spectrosc. Relat. Phenom. 153 (2006) 102.
[6] T.J.M. Zouros, O. Sise, M. Ulu, M. Doğan, Meas. Sci. Technol. 17 (2006) N81.
[7] O. Sise, T.J.M. Zouros, M. Ulu, M. Doğan, Meas. Sci. Technol. 18 (2007) 1853.
[8] O. Sise, T.J.M. Zouros, M. Ulu, M. Doğan, Nucl. Instrum. Methods Phys. Res. A, in print.
[9] O. Sise, T.J.M. Zouros, M. Ulu, M. Doğan, Nucl. Instrum. Methods Phys. Res. A, in print.
[10] T.J.M. Zouros, E.P. Benis, J. Electron Spectrosc. Relat. Phenom. 125 (2002) 221.
[11] T.J.M. Zouros, E.P. Benis, J. Electron Spectrosc. Relat. Phenom. 142 (2005) 175.
[12] M.E. Rudd, Electrostatic Analysers, in: K.D. Sevier (Ed.), Low Energy Electron Spectrometry, Wiley, New York, 1972, pp. 17–34.
[13] V.P. Afanas'ev, S.Y. Yavor, Sov. Phys. Tech. Phys. 20 (1976) 715 [Translation of Zh. Tekh. Fiz. 45 (1975) 1137–1170].
[14] E. Granneman, M.V. der Wiel, in: E.-E. Koch (Ed.), Handbook of Synchrotron Radiation, Vol. 1A, North Holland Publishing Company, Amsterdam, 1983, pp. 367–456.
[15] D. Roy, J.-D. Carette, Can. J. Phys. 49 (1971) 2138.
[16] S.D. Kevan, Rev. Sci. Instrum. 54 (1983) 1441.
[17] C.E. Kuyatt, J.A. Simpson, Rev. Sci. Instrum. 38 (1967) 103.
[18] F. Hadjarab, J.L. Erskine, J. Electron Spectrosc. Relat. Phenom. 36 (1985) 227.
[19] D.A. Dahl, J.E. Delmore, A.D. Appelhans, Rev. Sci. Instrum. 61 (1990) 607.
[20] D.A. Dahl, SIMION 3D v6. 0, Idaho National Engineering Laboratory, Idaho Falls, 1996.
[21] T.J.M. Zouros, O. Sise, F.M. Spiegelhalder, D.J. Manura, Int. J. Mass Spectr. 261 (2007) 115.
[22] E.P. Benis, T.J.M. Zouros, P. Richard, Nucl. Instrum. Methods Phys. Res. B 154 (1999) 276.
[23] E.P. Benis, T.J.M. Zouros, H. Aliabadi, P. Richard, Phys. Scr. T80 (1999) 529.
[24] E.P. Benis, et al., Phys. Rev. A 69 (2004) 052718.
[25] O. Sise, T.J.M. Zouros, M. Ulu, M. Doğan, NIMPRB, (2008), in press.
[26] B. Sulik, N. Stolterfoht, Auger Electron Spectroscopy of Target Atoms, in: S.M. Shafroth, J.C. Austin (Eds.), Accelerator-based Atomic Physics Techniques and Applications, American Institute of Physics Conference Series, New York, 1997, pp. 377–425.
[27] V. Schmidt, Electron Spectrometry of Atoms using Synchrotron Radiation, Cambridge University Press, Cambridge UK, 1997.
[28] T.J.M. Zouros, E.P. Benis, J.E. Schauer, in: J.L. Duggan, I.L. Morgan (Eds.), Application of Accelerators in Research and Industry, Vol. 576, American Institute of Physics, 2001, pp. 76–79 (AIP Conference Proceedings, New York).
[29] C.E. Kuyatt, Atomic and Electron Physics-Atomic Interactions, in: B. Bederson, W.L. Fite (Eds.), Methods of Experimental Physics, vol. 7A, Academic Press, New York, 1968, 1–43.

[30] F.H. Read, et al., J. Electron Spectrosc. Relat. Phenom. 4 (1974) 293.
[31] J.E. Pollard, D.J. Trevor, Y.T. Lee, D.A. Shirley, Rev. Sci. Instrum. 52 (1981) 1837.
[32] D.W.O. Heddle, Electrostatic Lens Systems, second ed., IOP, Bristol, 2000.
[33] J.H. Moore, C.C. Davis, M.A. Coplan, Building Scientific Apparatus, Addison-Wesley, London, 1983.
[34] N. Stolterfoht, Phys. Rep. 146 (1987) 315.
[35] T.J.M. Zouros, et al., Nucl. Instrum. Methods Phys. Res. B 40/41 (1989) 17.
[36] T.J.M. Zouros, D.H. Lee, in: S.M. Shafroth, J.C. Austin (Eds.), Accelerator-based Atomic Physics Techniques and Applications, AIP Press, Woodbury, NY, 1997, pp. 426–479.
[37] E.P. Benis, et al., Nucl. Instrum. Methods Phys. Res. B 146 (1998) 120.
[38] T.J.M. Zouros, et al., Phys. Rev. A 49 (1994) 3155.
[39] D.H. Lee, et al., Phys. Rev. A 41 (1990) 4816.
[40] T.J.M. Zouros, C.P. Bhalla, D.H. Lee, P. Richard, Phys. Rev. A 42 (1990) 678.